Citation
Cui, L. and Zhang, X. and Hao, H. and Zhang, X. 2022. Experimental investigation of resistance function of RC beam considering membrane effects. Engineering Structures. 267: 114602. http://doi.org/10.1016/j.engstruct.2022.114602

Experimental Investigation of Resistance Function of RC Beam Considering Membrane Effects

Liuliang Cui, Centre for Infrastructure Monitoring and Protection, School of Civil and Mechanical Engineering, Curtin University, Kent Street, Bentley, Australia, liuliang.cui@postgrad.curtin.edu.au

Xihong Zhang*, Centre for Infrastructure Monitoring and Protection, School of Civil and Mechanical Engineering, Curtin University, Kent Street, Bentley, Australia, xihong.zhang@curtin.edu.au.

Hong Hao, Centre for Infrastructure Monitoring and Protection, School of Civil and Mechanical Engineering, Curtin University, Kent Street, Bentley, Australia, hong.hao@curtin.edu.au.

Abstract

Membrane actions commonly exist in reinforced concrete (RC) elements under flexural deformation, which could significantly increase the ultimate flexural load-bearing capacity and potentially influence the damage mode of the RC element. Most design codes only treat membrane actions as a “hidden” safety factor without considering its influence on the resistance functions and failure modes. In this paper, an experimental investigation is conducted to study the membrane actions on the resistance behaviors of restrained RC beams. It is found that compressive membrane effect occurred at early stage of a fully restrained RC beam, which leads to amplified flexural bending resistance capacity. Diagonal shear crack is developed since the designed shear resistance is lower than the amplified flexural bending capacity. Under membrane actions, the damaged beam with shear crack could still carry the imposed load and develop further tensile membrane action until eventual failure. The resistance function of the restrained beam under combined membrane and shear damage is significantly altered as compared to the un-restrained reference beam that failed in flexural bending. A modified

theoretical resistance function is proposed to consider both the membrane effects and diagonal shear damage. Comparison with testing data shows that the proposed model could accurately describe the resistance of fully restrained RC beams under combined shear and membrane actions.

Keywords: reinforced concrete; restrained beam; membrane effects; diagonal shear; resistance function

1. Introduction

Deliberate terrorist bombing attacks, accidental explosions, vehicle and ship impacts on structures and facilites have been frequently reported, which impose substantial threats to the safety of people and property. For example, the 2014 accidental gas explosion in New York City [1] levelled two apartment buildings and caused 8 deaths and over 70 injuries; the 2020 Beirut explosion [2] caused at least 218 deaths, 7000 injuries, and billions of dollars of property damages. Thus, there is imminent demand for proper design and analysis of civilian structures to resist blast and impact loadings [3]. The current design analysis is based primarily on an equivalent single-degree-of-freedom (SDOF) model [4-7], in which the nonlinear response is modelled by load-deflection curve associated with the failure mechanism of the structure [8-12]. The accuracy of SDOF analysis strongly depends on the equivalent parameters, namely equivalent mass, stiffness, and load, which are determined from the actual structural and loading parameters and the expected structural deformation shape under the applied load. Most design codes, such as UFC 3-34-02 [13], assume a flexural dominant deformation mode and the nonlinear structural responses is modelled by a simplified bilinear elastic-perfectly-plastic resistance function, which nevertheless have been often demonstrated not always yielding accurate structural response predictions because both field and laboratory tests found the responses of a structural component may not necessarily be dominated by flexural response mode, but by shear or combined shear and flexural bending response mode. Furthermore, the bilinear elastic-perfectly-plastic resistance function neglects strain hardening and the membrane effect existing in restrained structures, which could significantly underestimate the structural load-resistance capacities [14-17]. Therefore, to more accurately predict the structural responses, it is necessary to generate more accurate resistance function (load-deflection curve) for design analysis.

Previous studies found the ultimate load-bearing capacity of restrained RC beams/columns against transverse loading and their response limit can be significantly enhanced by membrane effect [18-21]. Take a RC beam as an example without losing generality, compressive membrane action could be developed at early stage. When the beam deflects under the imposed transverse loading, initial longitudinal deformation would cause the beam edges to move outward and react against the stiff boundaries. An in-plane compressive membrane force is therefore induced. Because of the high axial stiffness, despite beam deformation is tiny, a considerable compressive force would be introduced, which increases the flexural strength of the beam sections at the yield lines. Thus, the ultimate load-bearing capacity of the beam would be substantially improved as compared to that without membrane effect. As the deformation grows, concrete cracks would gradually penetrate through the whole depth of the beam until its edges begin to move inward. If the edges of the beam are properly restrained, tensile membrane forces will be induced that enable the beam to carry much more load by the catenary action of the reinforcements. A typical load-deflection relationship for a restrained RC element considering membrane effects is illustrated in Fig. 1 [12].

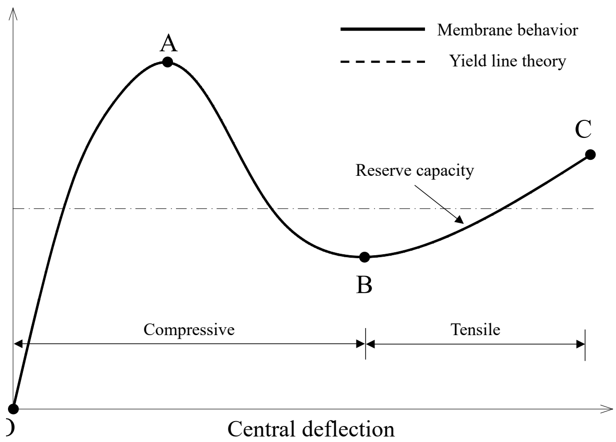

Fig. 1 Typical load-deflection relationship for fully restrained RC members considering compressive and tensile membrane effects.

To understand membrane effects on RC elements, some theoretical and experimental studies have been conducted [14, 20-24]. Ockleston [21] tested uniformly loaded full-scale reinforced concrete slab-and-beam floors on an existing multistorey dental hospital in Johannesburg. It was found that considerable compressive membrane action can be enforced by the stiffness of surrounding beams and panels. The ultimate loads of the three tested panels were more than twice of the ultimate loads predicted by yield line theory. Woodson [20] tested 16 one-way restrained RC slabs with uniformly distributed static pressure. It was observed that compressive membrane forces increased the ultimate capacities of the slabs for approximately 1.2 to 4.0 times of the computed yield-line resistance. It was demonstrated that the principal reinforcement significantly affects the membrane behaviors of one-way slabs. Chen et. al [24] carried out an experimental study on the membrane effects of hybrid fiber reinforced-lightweight aggregate concrete (HFR-LWC) beams, and discussed the influences of constraint stiffness, reinforcement ratio and fiber content on membrane actions. Generally, all the testing and analytical results have demonstrated that because of compressive membrane effect the ultimate load-bearing capacity of the slabs could be significantly (many times) higher than that predicted by the yield line theory. This is particularly apparent when the restraint at slab boundary is stiff and the reinforcement ratio is small. By considering the geometric compatibility and force equilibrium, Park and Gamble [18] proposed an equation to estimate the peak compressive membrane force. But their method requires a predefined mid-span deflection at the peak load to obtain the load-deflection relationship. Chen et al. [25] improved this equation by identifying three phases in the compressive membrane domain based on the flow theory, and derived the compressive membrane resistance curve without predetermining the deflection at peak load. Compared to the compressive membrane behavior that can increase the initial load-bearing capacity, tensile membrane behavior can be a significant factor in limiting the catastrophic failure and progressive collapse [26-29]. The increase in the load resistance capacity in the tensile membrane domain is often called reserve capacity. A reserve capacity could be very useful in the design of civilian structures against low probability but high consequence blast loading scenario, especially when it sustains large deflections with moderate-to-severe structural damage [7]. Park [30] developed an equation for describing the tensile membrane behavior, which assumes the load is carried mainly by reinforcing bars acting as tensile membranes when concrete cracks penetrate through the beam depth. But that equation is a straight line through the origin. In reality, as illustrated in Fig. 1 the tensile membrane behavior is activated from point B. Cui et al. [12] unified the compressive and tensile membrane actions, and modified the compressive membrane formulations and the transition into the tensile membrane domain to propose an improved analytical resistance model including both the compressive and tensile membrane behaviors. By employing the improved resistance model, a complete load-deflection curve (resistance function) can be depicted and adopted for structural dynamic analysis based on SDOF approach.

As described above, membrane effects comprise of both tensile membrane action when the structural component develops a large deformation (2nd effect), and also compressive membrane action when the component only experiences small deformation (non-secondary effect). Owing to the latter action, the ultimate flexural capacity of a RC beam could increase 1.5 to 2 times comparing to the design capacity without considering membrane action [7], which might lead to the flexural bending capacity higher than the shear capacity for a normally designed RC beam. In this case, shear failures might occur before flexural failure which is undesirable since shear failures normally exhibit fewer significant signs of distress and thus provides much less warnings than flexural failures [31, 32]. For most beams, the shear stresses may be below the direct shear strength of element, while diagonal shear failures are more prone to occur under the combined action of flexural and shear stresses. It is observed that for a simply supported beam, after the yielding of transverse reinforcements, the final diagonal shear failure of the beam follows either by splitting (dowel) failure or by compression zone failure [33]. However, such situations might not be devastating for elements with fully restrained boundary conditions since tensile membrane action could be induced to mitigate the total collapse of elements as long as their longitudinal reinforcements are adequately anchored and the integrity of support is not jeopardized [7]. This could make membrane effects much more attractive but more complex for analysis. There is no such study available yet.

Overall, despite the known benefits of membrane effects on increasing structural resistance capacity, existing studies are mainly focused on either the compressive membrane action or tensile membrane action. There are very limited studies available covering both the compressive and tensile membrane effects to fully depict the resistance function. And there is no study yet taking into account of the combined membrane effect and potential shear damage. This paper is devoted to performing an experimental study of the compressive and tensile membrane actions for better understanding the performances of fully restrained RC beams. Four RC beams are designed and fabricated, among which three beams are fully restrained to achieve membrane actions and one laterally unrestrained (reference) beam without membrane action. All beams are designed with longitudinal reinforcements extended and anchored into heavily reinforced concrete footings to achieve fully fixed boundary conditions. To ensure membrane effects, the footings of the three fully restrained beams are clamped to the strong floor to resist their longitudinal, transitional and rotational movements. For the reference beam, the longitudinal movement at the supports are not restrained. Three-point bending tests are performed to inspect the membrane effect and failure modes of the beams. Their influences on the load-bearing capacity of the beams are studied. Based on testing results and previous studies, a modified theoretical resistance function considering both membrane actions and combined shear damage mode is proposed.

2. Experimental Program

2.1. Specimen design

Four identical RC beams as shown in Fig. 2 are designed and fabricated following AS 3600 [34]. The beams are 2000mm long with cross section of 150mm×150mm. The longitudinal reinforcement in the beams consists of four N12 (12 mm diameter) steel rebars which are arranged symmetrically in the cross section of beam with concrete covering thickness of 20mm. It corresponds to a tension reinforcement ratio of $\rho = 1.32\%$ ($\rho = A_s/bd$, where A_s is the area of tensile reinforcement, b is the width of beam cross-section, d is the distance from extreme compression fiber to the centroid of tension reinforcement). The longitudinal reinforcements are continuous through the beam end into the two heavily reinforced concrete footings with the dimension of 750mm (height) × 500mm (length) × 300mm (width) and are bent and protruded through the top face of the footing and anchored using steel plates to provide sufficient anchorage. The transverse reinforcements having a diameter of 10 mm are spaced uniformly along the beam length with a spacing of 200mm.

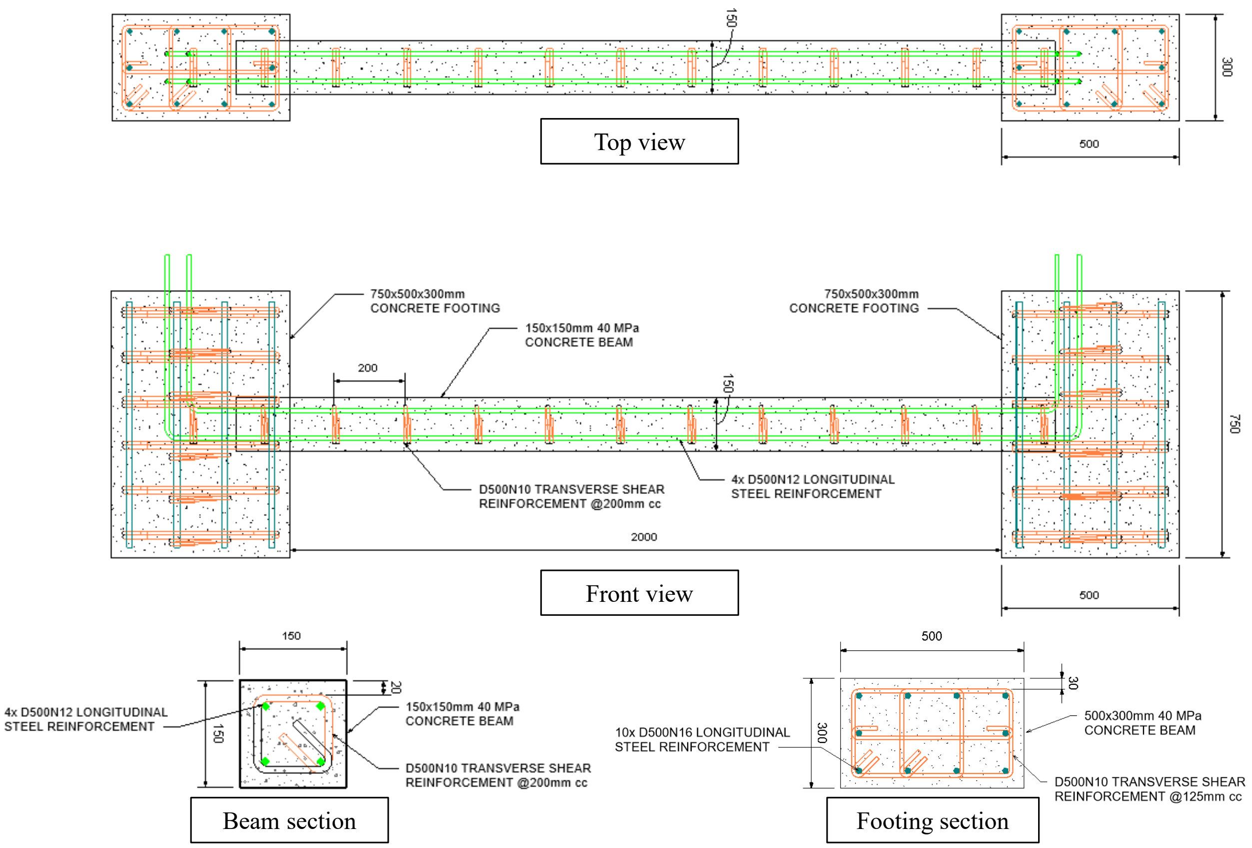

Fig. 2 Geometry and reinforcement arrangement of concrete beam specimens (unit: mm)

2.2. Reaction frame and test setup

As observed by other researchers [18, 20], the compressive membrane effect is sensitive to the lateral restraint stiffness. Considering the unavoidable discrepancies of specimen dimensions during manufacturing, the variation in lateral restraint stiffness in test setup (designed to be the same) as well as other uncertainties, in this test program, three replicated specimens (named as SM1, SM2, SM3) are prepared and tested to evaluate the compressive and tensile membrane actions. And a reference specimen (reference beam SC1) will be only restrained against rotational movements only therefore no membrane actions are expected.

In order to provide sufficient restraint, particularly in the longitudinal direction, for beams SM1, SM2 and SM3 to induce membrane forces, a reaction frame is specially designed and fabricated. Fig. 3 (a) shows the schematic view of the reaction frame. The left footing of the specimen is clamped on the strong steel reaction frame (100-ton capacity) in the laboratory by two rectangular hollow steel (RHS) beams (150mm×100mm×9mm RHS). The footing on the other side is restrained by a strong support made of heavy UB sections which are fully anchored onto the strong floor in the laboratory. Besides, four 20mm diameter Reidbars are introduced to connect these two strong supports along the longitudinal direction of the beam. As a result, the inward and outward longitudinal movements of the specimen are restrained. Two RHS beams are used to bolt the footings down to the strong floor through steel rods to restrain the rotational movement and uplifting. Additionally, to prevent the pull-out of longitudinal reinforcements as a result of the anticipated large tensile forces in the tensile membrane action, the longitudinal reinforcements are extended into the concrete footing and bent upwards. The protruding ends of the reinforcement are threaded and anchored using a 10mm steel plate (as shown in Fig. 3b). During the testing setup, all the above components of the reaction frame are fastened as strong as possible using a torque wrench. For the reference non-restrained beam SC1, the longitudinal restraint is set free by removing the end support from one end and the Reidbars as shown in Fig. 3 (c) and (d). As a result, the longitudinal movement of this reference beam is enabled. Thus, there is no restraint to induce compressive or tensile membrane forces to the beam.

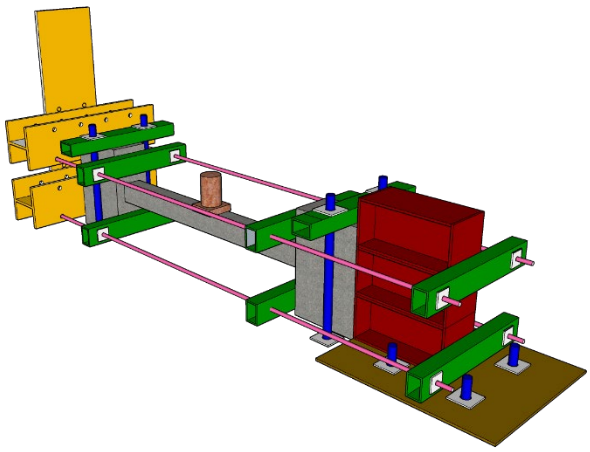

(a)

(b)

(c) (d)

Fig. 3 Test set-up and support conditions

2.3. Material properties

Table 1 lists the material properties of all reinforcements and Reidbars provided by suppliers. Both rebars have a yielding strength of 500MPa and an elastic modulus of 200GPa.

Table 1 Material properties of reinforcements and Reidbar

Material	Diameter (mm)	Yield strength (MPa)	Elastic modulus (GPa)
N10	10	500	200
N12	12	500	200
N16	16	500	200
Reidbar	20	500	200

Eight concrete cylinders (d=50mm, h=100mm) are prepared to measure its compressive strength and elastic modulus. The cylinders and the concrete beams are cured under ambient conditions. At 49 days when the formal test begins, the average compressive strength and elastic modulus of the concrete are found to be 41.37 MPa and 27.98 GPa, respectively. Five 100×100×500 mm concrete samples are also casted for determining the flexural tensile strength of concrete through four-point bending test. The obtained average flexural tensile strength of concrete is 4.02 MPa.

2.4. Test instrumentation

During the test, a concentrated static load is applied to the midspan of the beam by a hydraulic jack with a capacity of 200 kN. The loading rate is controlled at 2mm/min until the beam completely collapses. A load cell is instrumented to measure the applied force at mid-span of the beam. Five LVDTs (Linear Variable Differential Transformers) are installed along the top face of the beams to measure the deflections along the beam. Fig. 4 shows the layout of the LVDT (1-5), which are distributed along half of the span of the beam to depict the deflection shape. Besides, an additional LVDT (6) is used to record the longitudinal movement of the footing. A high-definition camera is set up in front of the tested beam to film its deformation-to-failure process under static loading. Because of the symmetry, only half of the beam is monitored. The video is post-processed using Digital Image Correlation (DIC) technique through the preprinted speckles on the specimens.

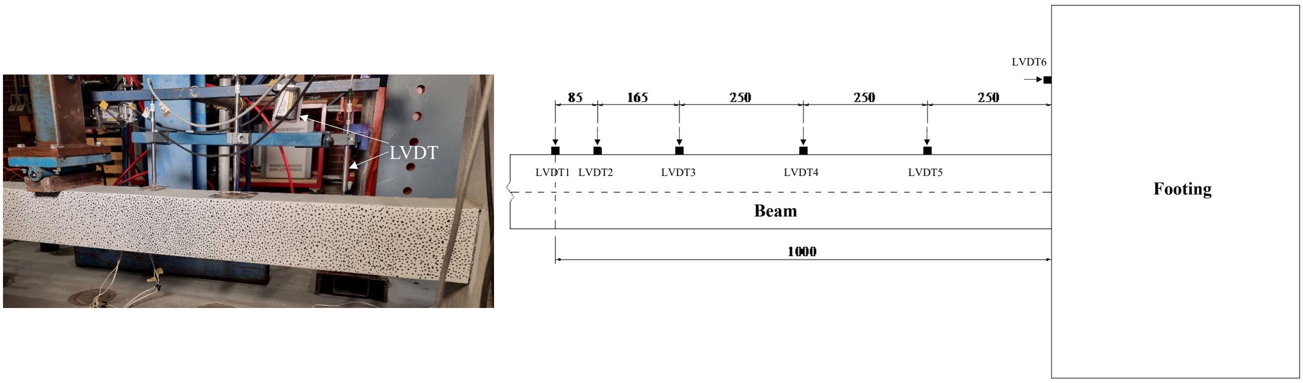

Fig. 4 Layout of LVDTs on the beam

3. Results and Discussions

All specimens are tested under concentrated transverse compression at mid-span until the total failure of the beam. The total failure of each beam is determined by the rupture of longitudinal reinforcements, which indicates no further tensile membrane force can be resisted by the reinforcements.

3.1. Damages of specimens

Fig. 5 shows the photos of the tested beams after the tests. As can be seen, the reference specimen SC1 without membrane effect fails by bending at both midspan and near the footings illustrating a three-hinged mechanism. Large vertical cracks appear at the bottom face of midspan and the upper face of supports, along with the concrete crushing in their opposite faces. In comparison, specimens SM1-3 exhibit combined shear and bending failures. Flexural cracks can be seen at midspan of the beam. Also, major diagonal shear cracks are developed near the supports of the beams. The reason why shear cracks are developed only on one side of the beam SM1 and beam SM2 might be because of the unavoidable manufacturing discrepancy

Based on the design parameters of the specimens and according to conventional design analysis without considering the membrane effect [35, 36], the failure of the beams should be governed by flexural bending with the predicted ultimate load corresponds to the flexural capacity of 46.7kN, and the shear capacity is around 65.2kN (1.4 times the flexural capacity). However, because of the activation of the membrane effect, the flexural capacity of SM1-3 is found to be greatly enhanced but their shear capacity is not increased significantly. As a result, diagonal shear cracks are developed in the fully restrained beams, and the failure modes of SM1-3 shift from flexural bending failure to combined shear and bending failure.

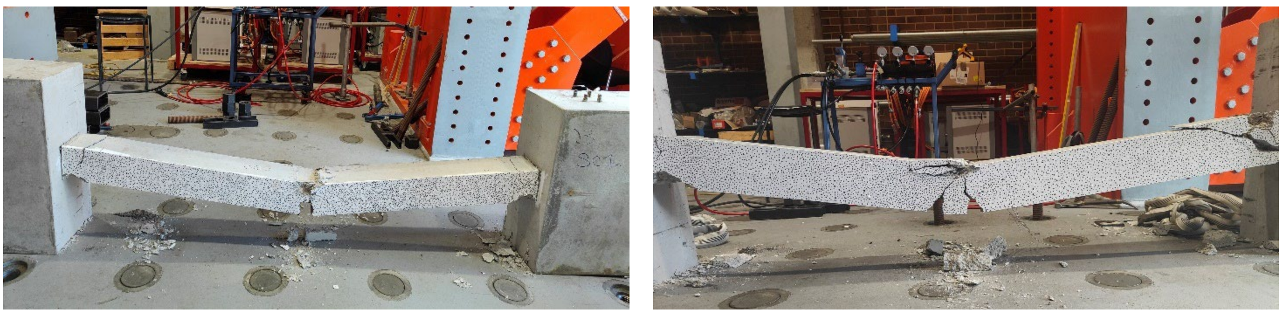

(a) SC1 (b) SM1

(c) SM2 (d) SM3

Fig. 5 Images of the tested beams.

3.2. Load-deflection curves

Fig. 6 shows the recorded load-deflection curves at midspan of the four specimens. Very apparent difference can be observed on the load-deflection curves between the fully restrained and unrestrained beams. For the reference specimen SC1, the load-deflection curve gradually rises with the applied concentrated loading to a peak of 56.62 kN with the corresponding midspan deflection of 24.52 mm. Afterwards, the load gradually decreases with further increased midspan deflection until the load suddenly drops due to the snap of the longitudinal reinforcement at midspan. The corresponding load is 41.56 kN. For the fully restrained specimens (SM1, SM2, SM3), the load-deflection curves rise much more rapidly than that of SC1 indicating much larger initial stiffness. The ultimate loads of SM1, SM2 and SM3 reach 70.9kN, 71.1kN and 69.1kN, with the corresponding midspan deflections of 13.8mm, 12.2mm and 15.9mm, respectively. Some discrepancies can be observed in the corresponding midspan deflections indicating variation in the stiffness of the ascending parts for SM1-3. This is because of the difference in the lateral restraint stiffnesses for these three beams that are unavoidable during installation. As derived by Cui et al. [12], the stiffness of lateral restraint could significantly influence the compressive membrane effect. The resistant loads then descend abruptly with a small displacement for all three specimens. It is also noted that very similar peak loads are achieved for SM1-3 since the diagonal shear failure occurs before it reaches the anticipated ultimate load owing to the compressive membrane action.

This phenomenon usually signifies the failure of the RC beam because of the loss of loading stability. Interestingly, these restrained specimens do not lose their bearing capacity completely after the occurrence of major shear cracks but maintain to resist a medium level load-resistance capacity for a long period, and then starts to increase again at large displacement. This is an indication that tensile membrane forces are developing within the beams. Overall, the load-deflection curves of SM1, SM2, and SM3 are very similar to each other. Specimen SM2 fails completely before the ultimate failure of the other restrained specimens. This could be attributed to the pre-existing defects in the longitudinal rebars as a result of grinding on the surface for placing the strain gauges. It leads to the early rupture of the reinforcement but as can be seen in the load-deflection curve this imperfection does not influence the initial behavior and the compressive membrane effect in the beam.

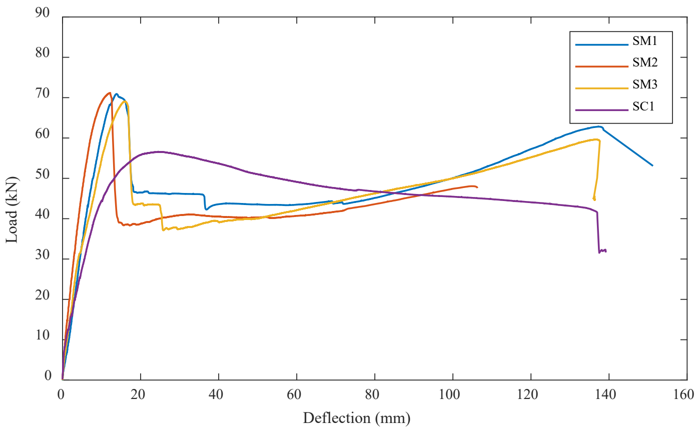

Fig. 6 Load-deflection curves at midspan of different specimens

Table 2 Summary of load-deflection data from experiment

Specimen No.	SC1	SM1	SM2	SM3
Ultimate load R_u (kN)	56.5	70.9	71.1	69.1
Def. at ultimate load D_u (mm)	24.9	13.8	12.2	15.9
Failure load R_f (kN)	41.5	62.8	48.1	59.6
Def. at failure load D_f (mm)	137	137.4	105.3	136.9
Ref. resistance R_r (kN)	46.7	46.7	46.7	46.7
$R_u/R_{u, SC1}$	1.00	1.25	1.26	1.22
R_u/R_r	1.20	1.52	1.52	1.48

Note: Ref. resistance R_r is the reference resistance predicted following CSA A23.3-2004 [36].

As can be seen from Fig. 6 and Table 2, the ultimate loads of the fully retrained beams (SM1-3) are significantly higher (+26%) as compared to the unrestrained reference beam. The enhancement of load-bearing capacity in this stage is attributed to compressive membrane action. Following CSA A23.3-2004, the ultimate load-bearing capacity of the RC beams with fully fixed supporting conditions is predicted to be 46.7kN (shown as the reference resistance R_r in Table 2). In comparison, the average loading capacity of the tested restrained beams is 51% higher than the code predicted ultimate load-bearing capacity, which implies that the commonly used design standards could significantly underestimate the load-bearing capacity of fully clamped RC beams when the transitional and rotational movements at the supports are restrained. It is also noted that the load-bearing capacity of the unrestrained reference beam is also 20% greater than the predicted resistance R_r. This is possibly because the vertical boundary restraint on the footings seem to not only provide rotational and vertical restrains, but also cause significant friction between the concrete footing and the strong floor which leads to additional longitudinal resistance. It can be seen in Fig. 5 (a) that there is some spalling of concrete near the bottom of the right footing of SC1. These resistances induce axial compressive forces in the beam, which as a result increases the flexural capacity of the reference beam. This observation and data coincident with Park and Gamble's observation [18] that even very small support stiffness can provide unignorable compressive membrane enhancements of the structural element.

3.3. Deformation-to-failure process

To further investigate the response of fully restrained RC beams with membrane effects and combined flexural bending and shear failure, the deformation-to-failure processes of the beams are analyzed with the DIC results. Typical load-deflection curve for the fully restrained beam SM1 and the unrestrained beam SC1 are compared.

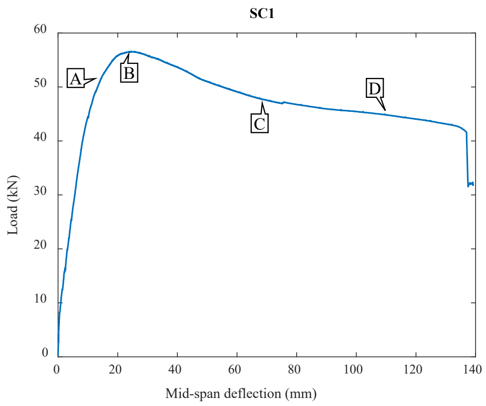

(a)

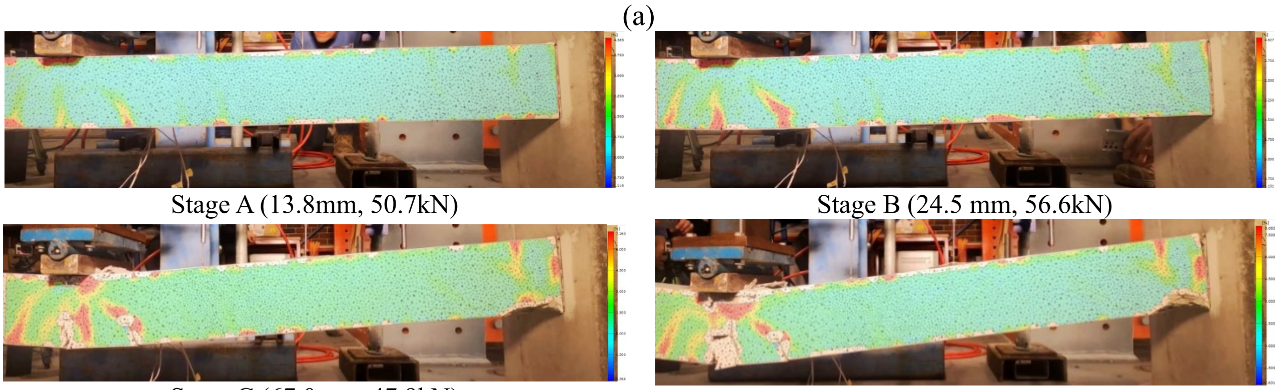

Stage A (13.8mm, 50.7kN)
Stage B (24.5 mm, 56.6kN)
Stage C (67.0mm, 47.9kN)
Stage D (110.0mm, 44.8kN)

(b)

Fig. 7 Load-deflection curve with major strain contour of the reference beam SC1

In Fig. 7 the load-deflection curve of the unrestrained beam SC1 is highlighted at critical stages, with the corresponding strain contours from DIC analysis. At stage A prior to reaching the peak load of the curve, flexural bending cracking begins to initiate from the bottom tensile region of the beam at midspan. At stage B of 24.4mm deflection, more flexural cracks at midspan can be observed, which widen and quickly extend upwards, with associated flexural microcracks becoming more visible near the support. At stage C major flexural cracking penetrates the full depth of the specimen at midspan with the vertical deflection of 67.0 mm. Additionally, crushing and spalling of the concrete can be observed on the top side of the midspan and the bottom of the beam at the supports. Prior to the complete failure of the beam, at stage D more severe cracking and crushing of the concrete at midspan can be seen corresponding to a large vertical deflection of 110.0 mm. It can be seen from the DIC analysis, there is no sign of shear cracks throughout the loading process. The DIC in conjunction with the corresponding load-deflection curve of SC1 illustrates the typical flexural tension failure of the fixed-end beam with the boundary unrestrained. This verifies the assumed failure mode in design code AS3600. The crushing and spalling of the concrete in these images evidence the occurrence of concrete softening, resulting in the gradual decrease in load resistant capacity after the peak in the load-deflection curve.

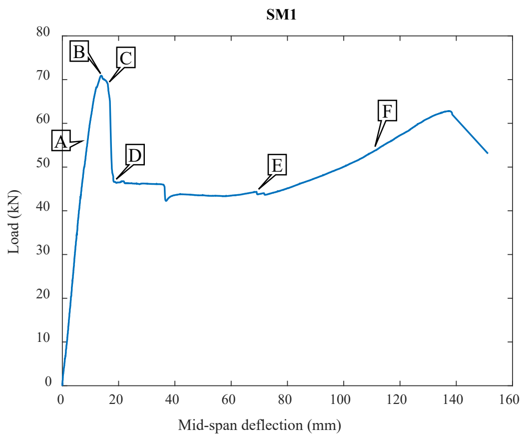

(a)

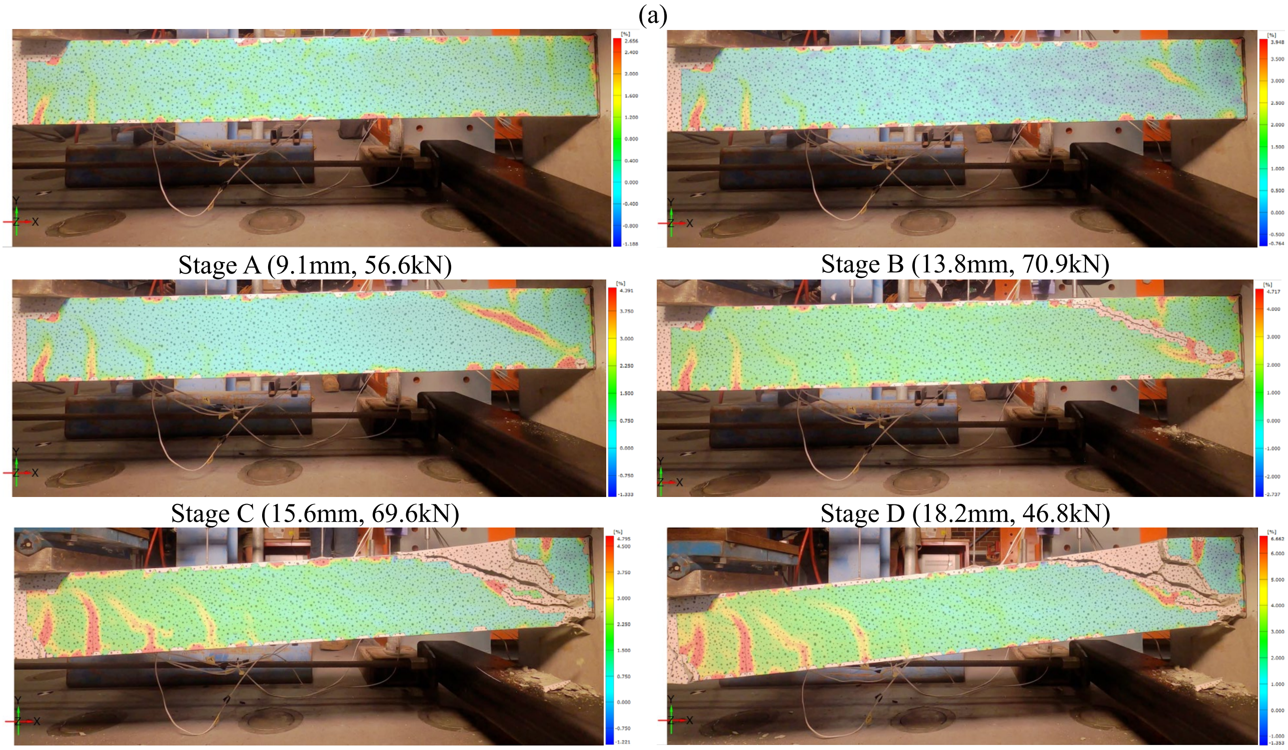

Stage A (9.1mm, 56.6kN)

Stage B (13.8mm, 70.9kN)

Stage C (15.6mm, 69.6kN)

Stage D (18.2mm, 46.8kN)

Stage E (67.0mm, 44.1kN)

Stage F (110.0mm, 53.3kN)

(b)

Fig. 8 Load-deflection curve with major strain contour for the fully restrained beam SM1

Comparing to the unrestrained beam, the response of the fully restrained beam SM1 is more complex due to the membrane effect. It can be seen from Fig. 8 that at Stage A as load reaches 56.6kN, concrete crack begins to initiate on the tensile face at midspan of the beam. Comparing the crack patterns between SC1 and SM1, it is apparent that the crack width and length in beam SC1 are much larger than those in SM1. Right before reaching the peak load at point B concrete cracks in the beam gradually extend. Initiation of diagonal shear crack is captured by DIC near the support. At stage C, right after reaching the peak load, the shear crack quickly propagates along the diagonal direction. Then, the shear crack penetrates the entire depth of beam SM1, and the load declines drastically within a very short displacement. At stage D, the load decreases to 46.8kN and the major shear crack is developed. As the beam SM1 is further loaded, flexural cracks at midspan and the diagonal shear crack near the support further increase, but the load only fluctuates without noticeable decrease or increase until point E when the load begins to increase again at about 67mm midspan deflection. Severe crack is developed at stage F with a midspan deflection of 110mm shortly before the complete failure of the specimen. In summary, in the initial loading state, the stiffness of the restrained beam SM1 is a lot larger than the control beam because of the existence of compressive membrane force, hence there are less and smaller cracks in SM1 under the same load. After the initiation of diagonal shear cracks in SM1, the number and size of vertical flexural cracks begin to increase quickly indicating that during stage D and E the deformation in the middle part of beam SM1 is still flexural dominant. After stage E, tensile membrane behavior is induced, flexural cracks in SM1 do not change much. Interestingly, there are more flexural cracks in SM1 than that in SC1. In other words, it implies that the deformation shape of SM1 differs from that of SC1 where a plastic hinge is formed at the mid-span section of the beam. This observation is helpful in studying the deformation shape function of beams under combined flexural and shear damage.

3.4. Support movement

Since the restraint at supports provide compressive and/or tensile membrane forces to the deformed specimens, the movement of supports could also be used to analyze the membrane actions. Fig. 9 shows the relationship between the longitudinal movement of the right hand-side support versus the measured beam midspan deflection during tests. Both the restrained and unrestrained specimens are presented for comparison, where positive and negative displacement referring to the outward and inward movement of the support, respectively. It can be seen that for the unrestrained reference beam SC1, the concrete footing moves outward as far as 4mm with the deflection of the beam. This is because at small transvers deflection, concrete cracking will cause the projection length of beam in the longitudinal direction to increase which pushes the unrestrained footing to move outwards. As transvers deflection increases beyond a certain value, the projection length begins to decrease, so the concrete footing moves inwards. It is evident that much smaller lateral movements are found on the restrained beams (SM1-3) where the measured maximum footing movements are all less than 0.5mm outwards. It can also be noticed that with reference to Fig. 6, the peak longitudinal movement of the footings for the fully restrained beams directly correlate to the instance of reaching the peak ultimate loads or the occurrence of shear damage. This is expected because the longitudinal movement of the concrete footing is mostly depending on the flexural deformation of the beam, while the major shear cracks greatly interfere the bending behaviors of the beam. Through comparing the maximum longitudinal movement of footings of the restrained beam with that of the unrestrained reference beam, it can be found that the designed reaction system works well in restraining support movement and thus inducing membrane actions.

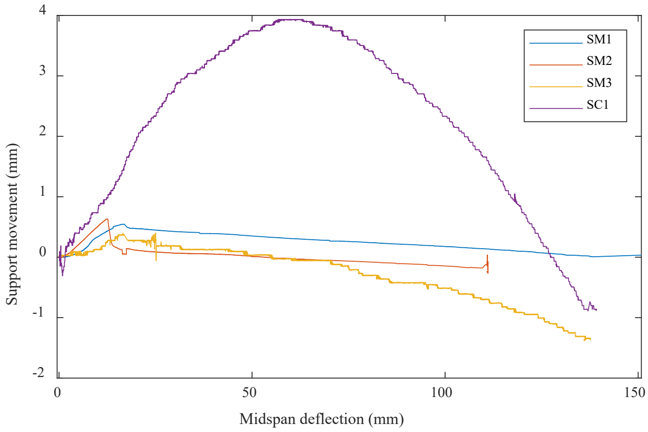

Fig. 9 Comparison of longitudinal movements of the right hand-side supports between the restrained and unrestrained beams

4. Modified Resistance Function

As discussed above, because of the membrane effect the flexural bending resistance of the RC beams is amplified which outweighs the shear capacity, the failure of the RC beam therefore changes from flexural failure to a combined flexural bending and diagonal shear failure. Conventionally designed RC components neglecting membrane effect would lead to a very conservative prediction of the member flexural resistance capacity, which in the meanwhile could lead to a different failure mode. Therefore, a proper resistance function model (load-deflection curve) is needed for properly and accurately prediction of the response of RC components.

Recently, Cui et al. [12] proposed an improved theoretical resistance function considering both the compressive and tensile membrane actions (as shown in Fig. 10a). Through comparing with previous testing data, this model was proved to be capable of accurately depicting the whole membrane behaviors of RC component. However, this model was established based on flexural failure mode where shear deformation was not considered. For fully restrained RC beams with combined flexural bending and diagonal shear failures, there is a sudden drop of load-bearing capacity on the load-deflection curve because of the diagonal shear failures. From the testing data and analysis in chapter 3, the load-deflection curve for RC component with membrane effect and combined flexural bending and shear failure modes can be modified and depicted as illustrated in Fig. 10b. Due to shear damage the full compressive membrane effect on load-carrying capacity may not be achieved, i.e., if the shear capacity of the beam is lower than the amplified flexural capacity of the beam with compressive membrane effect, the beam would fail by shear with a sudden drop in the load-resistance function. As the deflection and damage continue to increase, the load resistant capacity would maintain with further deformation and concrete damage until the tensile membrane action coming into effect. Then, the load resistant capacity starts to increase again as the deflection further increases. Accordingly, a modified theoretical resistance function accounting for diagonal shear effect can be sketched with a piecewise curve $OA_sB_sC_sD_s$ as shown in Fig. 10b.

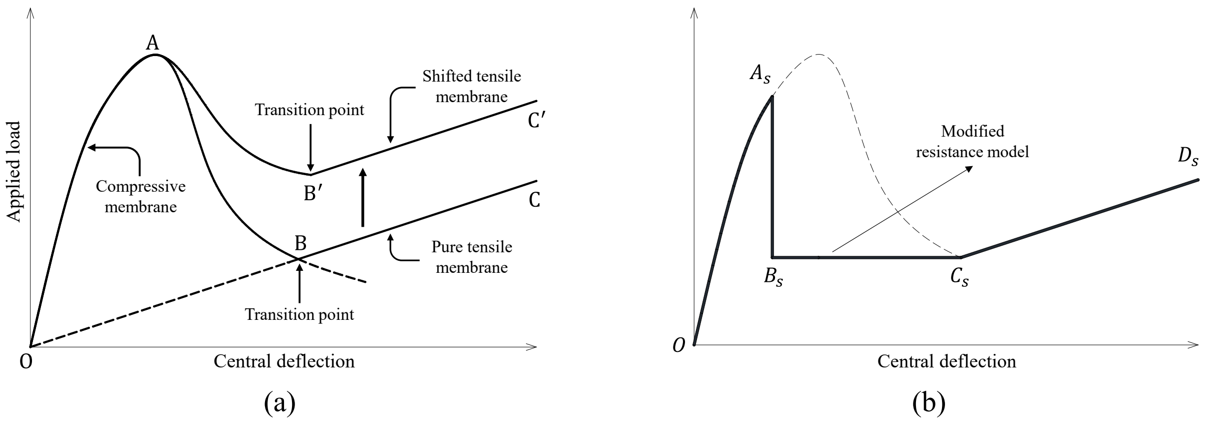

Fig. 10 (a) Compressive-tensile membrane resistance model proposed by Cui et al. [12]; and (b) the modified resistance model accounting for both membrane effect and diagonal shear damage

4.1. Modified compression field theory (MCFT) and determination of point A_s

As discussed before, the load of point A_s is correlated to the diagonal shear capacity of the RC element. It is worth noting that although determining the shear strength of RC beams has been discussed for decades, the predictions of shear strength by different design standards for a particular beam section can still vary by factors of more than 2 [33]. There are two major shear strength prediction models, i.e. the truss model adopted by ACI 318-14 [37] and the Modified Compression Field Theory (MCFT model) [35] adopted by the Canadian code CSA A23 [36]. The truss model assumes that after concrete cracking, the behavior of a RC element is similar to that of a truss with a top longitudinal concrete chord, a bottom longitudinal steel chord (consisting of longitudinal reinforcement), vertical steel ties (stirrups), and diagonal concrete struts inclined at 45^o. It assumes that the diagonally cracked concrete cannot resist tension and the shear force is resisted by transverse steel, commonly referred to as the steel contribution (V_s) and the uncracked concrete contribution (V_c). Unlike the truss model, the MCFT model assumes that a diagonal compression field carries the shear force after concrete cracking. The cracked concrete can be treated as a new material with empirically defined stress-strain behavior. The stresses and strains used in the stress-strain relationships are average stresses and strains. That is the combined effects of stresses and strains at cracks, between cracks, interface shear on cracks and dowel action are considered simultaneously. Besides, the MCFT model uses the strain conditions in the web to determine the inclination angle θ of the diagonal compressive stresses. These assumptions allow the MCFT model to consider the combined efforts of flexure, shear, axial load (compression or tension), and torsion, which is thus more suitable to current situation. Fig. 11 gives the equations of the MCFT model employed to predict the diagonal shear capacity (point A_s) for RC beams. The computer code Response-2000 [35] is employed in this study to quickly calculate the value, in which the design parameters and the combinations of the axial load, moment and shear force are used as inputs. The ratio between moment and shear stress can be easily determined, and the ratio between the moment and axial stress can be estimated by the membrane model proposed by Cui et. al [12].

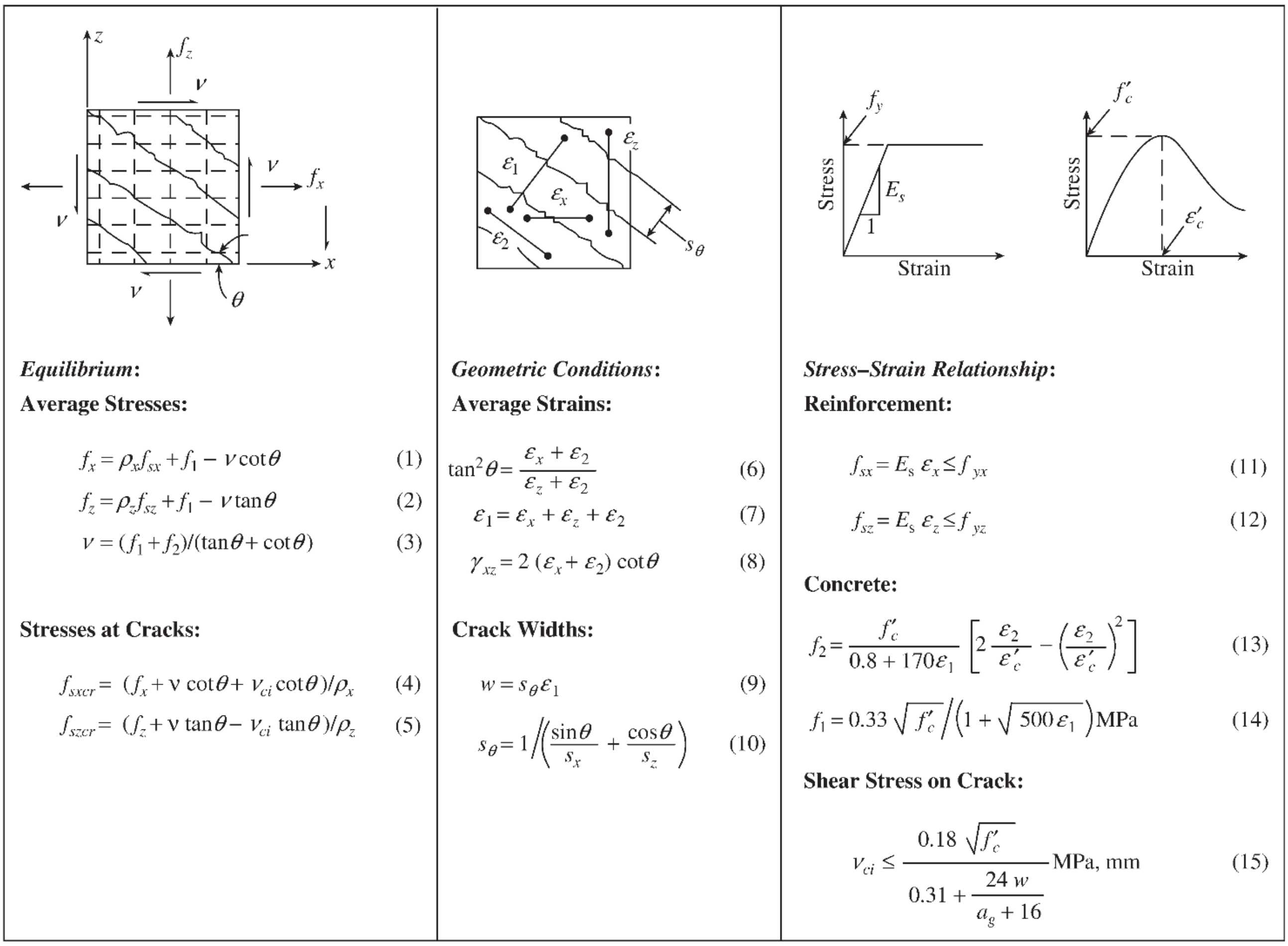

Fig. 11 Equations for determination of diagonal shear capacity from the MCFT model [35].

In Cui et al.'s model, the compressive membrane force-deflection relationship can be expressed as

$$\frac{dN}{df} = \frac{(\eta_S + \eta_M)h\frac{1}{0.5L} - f\frac{1}{0.5L}}{\frac{1}{S_n} + \frac{0.5L}{E_c bh + E_s(A_s + A_{ss})}} \tag{16}$$

in which

$$\eta_S h = 0.5h - x_n^S \quad \text{and} \quad \eta_M h = 0.5h - x_n^M \tag{17}$$

where N represents the compressive membrane force; f is the mid-span deflection of the beam; S_n is the lateral stiffness of supports; ρ is the reinforcement ratio; E_c and E_s are the elastic modulus of concrete and reinforcements; x_n^S and x_n^M are the depth of the neutral axis (depth of compressive zone) of the cross sections at supports and midspan, respectively; A_s and A_{ss} are the area of reinforcements in tension and compression respectively; L, h, b are the length, depth and width of the beam; I_a is the averaged moment of inertia of the beam. Therefore, the membrane force N can be obtained by solving this integration equation. Known the relationship between compressive membrane force and deflection, the following force equilibrium equation must be fulfilled at each instant

$$N+\sigma_s A_s-\sigma_{ss}A_{ss}-\sum_{i=1}^{i=n}\sigma_{ci}A_{ci}=0 \tag{18}$$

where the concrete is discrete into numbers of layers for analysis, and the tensile strength of concrete is neglected; n is the number of concrete layers in compression; σ_{ci} is the compressive stress of the *i* th layer of concrete; A_{ci} is the area of the *i* th layer of concrete; σ_s and σ_{ss} are the stresses in the tensile and compressive reinforcements. Taking moment about the neutral axis, the resultant moment M_R can be calculated as

$$M_R=\sigma_{ss}A_{ss}(\frac{h}{2}-d_c)+\sigma_s A_s(h_0-\frac{h}{2})+\sum_{i=1}^{i=n}\sigma_{ci}A_{ci}y_{ci} \tag{19}$$

where d_c is the depth of the concrete cover; h_0 is the effective depth; and y_{ci} is the distance from the *i* th layer of concrete to the neutral axis. For a restrained beam under concentrated load, the load-carrying capacity *q* can be computed by

$$q=\frac{8}{L^2}(M_R^S+M_R^M-Nf) \tag{20}$$

where M_R^S and M_R^M are the resistant moments at supports and midspan. Therefore, the resistance curve considering compressive membrane action only (curve OAB or OAB') can be derived through equations (16)~(20), as shown in Fig. 10a. If the predicted shear capacity is larger than the calculated enhanced flexural capacity, the beam would be flexural dominant, and the resistance curve would be OABC or OAB'C' that can be derived using Cui et al's model in reference [12]. If the predicted shear capacity is smaller than the enhanced flexural capacity, the original resistance curve would be replaced by curve $OA_sB_sC_sD_s$. The determination of points points B_s, C_s, and D_s will be discussed in the next section.

4.2. Determination of points B_s, C_s, and D_s

The transition point B (B') represents the instance when the membrane force changes from compression to tension. It is determined to be the intersection point between the pure tensile membrane line and the descending branch of the compressive membrane curve or the lowest point of the compressive membrane curve if they do not intersect. The expression for the pure tensile membrane line is

$$q_T = 4T_y f/L \tag{21}$$

where T_y is the yielding force of the reinforcement per unit width; and L is the clear span length. It is a straight line OBC as shown in Fig. 10a, which will shifted from the transition point B to B' to form the tensile membrane line B'C' if it does not intersect with the compressive membrane curve at B'. Compared to Cui et al.'s model, point Cs in the modified resistance model in Fig. 10b also signifies the beginning of tensile membrane action. It is reasonable to consider that point Cs coincides with point B (B'). Since point Bs in the modified resistance model shares the same load-bearing capacity of point Cs, and it is considered to have the same deflection as point As, after the determination of point As and Cs, point Bs can be determined automatically.

The determination of points B_s and C_s can be justified by the analysis of experimental observations. After point A_s, despite the major diagonal shear crack, the beam still maintains a good integrity and continues to resist the imposed load providing that the longitudinal reinforcements are properly anchored into the footing. Therefore, the shear force and bending moments can still be transmitted along the beam length through the longitudinal and multiple cohesive stress from transverse reinforcements, aggregates and uncracked concrete [38]. However, the major diagonal shear crack on concrete would significantly influence the transmitting of axial compression. Thus, the compressive membrane action will be released quickly. As evidenced in Fig. 9, when shear crack occurs, the outward movement of support suddenly plumets, and then begins to gradually move inward. This phenomenon indicates that the compressive membrane force drops when diagonal shear crack develops. The sudden loss of the large compressive membrane force would greatly alter the stress distribution at the cross section and thus reduce the load-bearing capacity of the beam as illustrated in Fig. 6. Therefore, the bearing capacity at this stage (B_s) should be close to the transition point where the compressive membrane force becomes zero. As beam deflection further increases, the bearing capacity would not change significantly because of stress redistribution until concrete crushes and cracks penetrate through the entire depth of the beam section. At this instance, concrete is completely out of work. Due to the large bending curvature of the longitudinal reinforcements, the plane-section assumption is no longer valid. The load-bearing mechanism changes from the Bernoulli beam mechanism into the catenary mechanism. Afterwards, the load-bearing capacity of the beam increases with the growth of beam deflection as a result of tensile membrane effect. Therefore, point C_s can be regarded as the transition point of compressive membrane effect into tensile membrane effect.

The failure point D_s depends on the ductility of the longitudinal reinforcement. Based on UFC3-340-02 [13], if sufficient lateral restraint is provided, the mid-span deflection corresponding to support rotations of 8 degree is considered as the limiting deflection of beams under tensile membrane action. Assuming it is a straight line between the beam end and its midspan, the limiting mid-span deflection f_{lim} (deflection of point D_s) can be estimated by

$$f_{lim} = L/2 \cdot (8\pi/180) \tag{22}$$

Therefore, the complete modified resistance model can be derived following the procedure discussed above. Fig. 12 illustrates the flow chart for determining the resistance functions of a restrained RC element considering both the compressive and tensile membrane effects, as well as the potential shear damages.

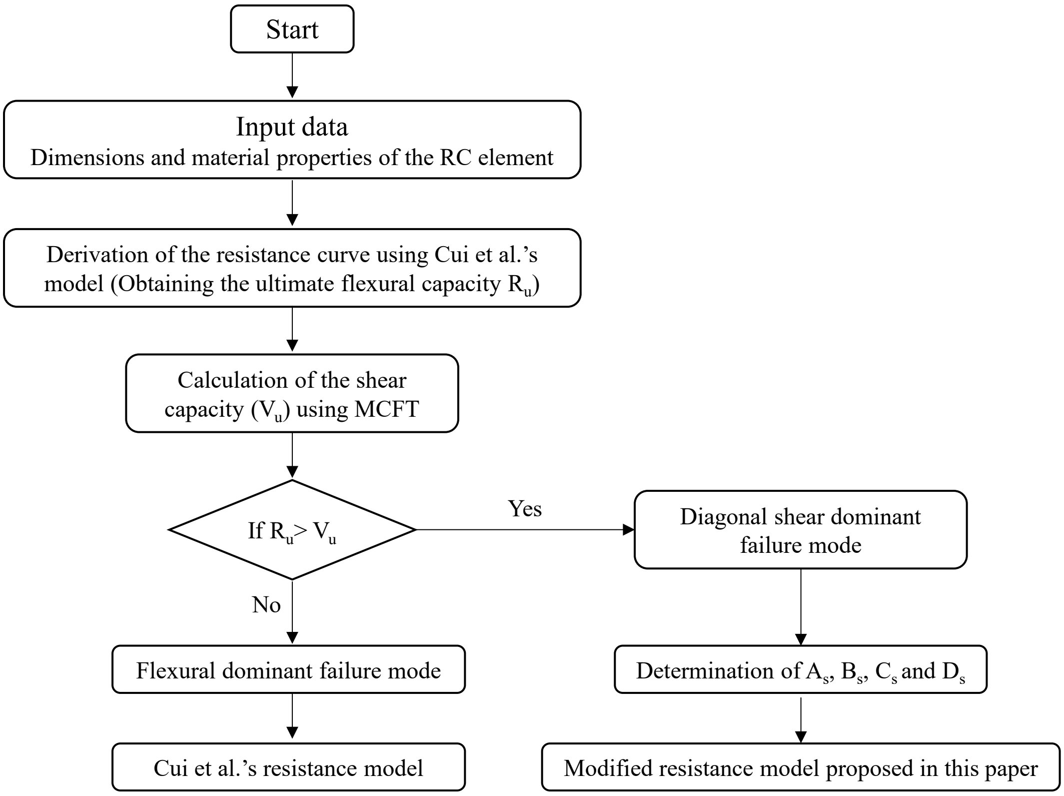

Fig. 12 Flow chart for determining the resistance functions of restrained RC beams

4.3. Model verification

To verify the accuracy of the modified resistance function model, the testing results in this study is employed to compare with the prediction using the proposed theoretical model. Based on the design parameters of the RC beams as detailed in chapter 2, the resistance function can be derived as shown in Fig. 13. The pink dashed-dot line is the resistance function considering membrane effects predicted using Cui et al.'s model. The modified resistance function considering both the membrane effect and the combined flexural bending and shear failure mode is shown as the black dashed line. Based on the MCFT, the peak resistance load (A_s) in the modified model is 75.6 kN corresponding to a deflection of 11.3mm, of which the load is slightly higher (+7.4%) than the averaged ultimate load 70.4 kN obtained from the tests. The predicted deflection is -20.3% smaller than the averaged deflection of 14.0 mm from the test. This is probably because of the unavoidable support movement (0.5mm) in the tests which leads to a smaller compressive membrane force and larger deflection of beam.

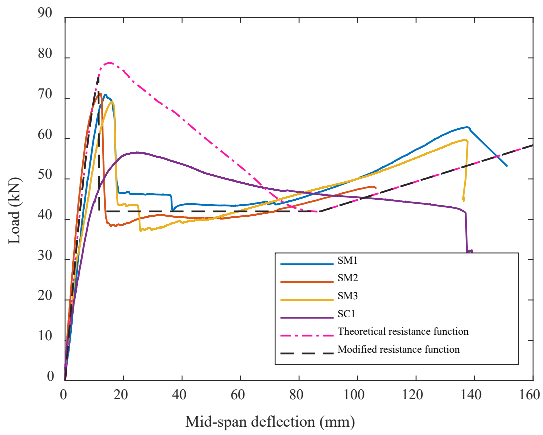

Fig. 13 Comparison of the modified resistance function and the testing results

In the modified resistance function model, the valley load (B_s) after the peak is 42.1 kN which is almost the same as the averaged tested value of 42.9 kN. The resistance maintains constant until reaching the predicted transition point (C_s) to tensile membrane domain which is around the deflection of 87 mm. The average load recorded in the test at this deflection is about 46.4 kN, which is 10.2% higher than the prediction of the modified resistance function model. Finally, the predicted ultimate load and the limiting deflection of D_s are 53.9kN and 140.5mm respectively, which are only -11.9% lower and +2.6% higher than the testing result. Table 3 compares the model prediction and testing results. Overall, from the above comparison, it can be found that the modified resistance function model could closely predict the resistance function of the fully restrained RC beam with consideration of both compressive and tensile membrane effects, as well as the combined diagonal shear and flexural bending failure modes.

Table 3 Test and model predicted results

Items	Peak load (kN)	Def. at peak load (mm)	Valley load (kN)	Load of the transition point (kN)	Ultimate load (kN)	Limiting Def. (mm)
Averaged test result	70.4	14.0	42.9	46.4	61.2	137.0
Modified	75.6	11.3	42.1	42.1	53.9	140.5

resistance model	(+7.4%)	(-20.3%)	(-1.9%)	(-10.2%)	(-11.9%)	(+2.6%)

Note: value in parenthesis is the prediction error with respect to the test result

5. Conclusion

In this study, experimental study is carried out to investigate the response of RC beams with compressive and tensile membrane actions. Three-point bending tests are conducted on four RC beams. Comparing to the reference unrestrained beam which develops typical flexural bending failure mode, three fully restrained beams develop a combined diagonal shear and flexural bending failure mode, and evident compressive and tensile membrane actions are observed. Analysis on testing data shows that compressive membrane action increases the beam bending capacity which outweighs their shear capacity and results in the formation of diagonal shear damage in the restrained RC beams. Nevertheless, because of the proper anchorage of longitudinal reinforcements in the restrained beams, they still maintain a considerable load capacity after the shear damage and continue to develop significant tensile membrane action with extra reserve capacity.

The test results show that for a normally designed RC beam (strong in shear and weak in bending) without considering the membrane effects, its bending capacity can be overly underestimated. Besides, a flexural governed beam may suffer shear damage because the membrane effects could amplify flexural capacity of the beam that outweighs its shear capacity. Even if the brittle shear damage occurred, as long as the RC element is properly anchored, its resistance could still possibly maintain and develop reserved load-bearing capacity due to tensile membrane action.

To better describe the resistance behavior of the RC beam under the combined effects of membrane actions and shear damage, a modified theoretical resistance function model is proposed based on the analysis of experimental observations and previous studies. Through comparing with the testing results obtained in this study, it is found that the proposed model can provide accurate predictions of the resistance function of the restrained RC beams with membrane actions and potential shear damages.

Acknowledgement

The authors would like to acknowledge the financial support from Australian Research Council under Discovery Project fund DP190103253.

References

[1] Wikipedia. 2014 East Harlem gas explosion. https://en.wikipedia.org/wiki/2014_East_Harlem_gas_explosion2014.

[2] Wikipedia. 2020 Beirut explosion. 2020.

[3] Baker WE, Cox PA, Kulesz JJ, Strehlow RA, Westine PS. Explosion hazards and evaluation: Elsevier; 2012.

[4] Biggs JM. Introduction to structural dynamics. New York: McGraw-Hill Book Company; 1964.

[5] Low HY, Hao H. Reliability analysis of direct shear and flexural failure modes of RC slabs under explosive loading. Engineering Structures. 2002;24:189-98.

[6] Carta G, Stochino F. Theoretical models to predict the flexural failure of reinforced concrete beams under blast loads. Engineering Structures. 2013;49:306-15.

[7] Krauthammer T. Modern protective structures: CRC Press; 2008.

[8] Hao H. Predictions of structural response to dynamic loads of different loading rates. International Journal of Protective Structures. 2015;6:585-605.

[9] Burrell RP, Aoude H, Saatcioglu M. Response of SFRC Columns under Blast Loads. Journal of Structural Engineering. 2014;141:04014209.

[10] Wu C, Oehlers DJ, Rebentrost M, Leach J, Whittaker AS. Blast testing of ultra-high performance fibre and FRP-retrofitted concrete slabs. Engineering Structures. 2009;31:2060-9.

[11] Cui L, Zhang X, Hao H. Improved analysis method for structural members subjected to blast loads considering strain hardening and softening effects. Advances in Structural Engineering. 2021:13694332211007382 %@ 1369-4332.

[12] Cui L, Zhang X, Hao H, Kong Q. Improved resistance functions for RC elements accounting for compressive and tensile membrane actions. Engineering Structures. 2022;251:113549.

[13] UFC3-340-02. Structures to resist the effects of accidental explosions. Washington DC, Unified Facilities Criteria. 2008.

[14] Keenan WA. Strength and Behavior of Laced Reinforced Concrete Slabs Under Static and Dynamic Load, US Naval Civil Engineering Lab, R620. 1969.

[15] Krauthammer T, Bazeos N, Holmquist T. Modified SDOF analysis of RC box-type structures. Journal of Structural Engineering. 1986;112:726-44.

[16] Chen W, Luo L, Guo Z, Wang Y. Load-Carrying Capacities of Fully Clamped RC Slab Accompanying Compressive-Tensile Membrane Actions: A Theoretical Approach. International Journal of Structural Stability and Dynamics. 2020;20:2050094 %@ 0219-4554.

[17] Astarlioglu S, Krauthammer T, Morency D, Tran TP. Behavior of reinforced concrete columns under combined effects of axial and blast-induced transverse loads. Engineering Structures. 2013;55:26-34

[18] Park R, Gamble WL. Reinforced concrete slabs. New York: John Wiley & Sons; 2000.

[19] Christiansen KP. The effect of membrane stresses on the ultimate strength of the interior panel in a reinforced concrete slab. The Structural Engineer. 1963;41:261-5.

[20] Woodson SC. Effects of shear reinforcement on the large-deflection behavior of reinforced concrete slabs. ARMY ENGINEER WATERWAYS EXPERIMENT STATION VICKSBURG MS STRUCTURES LAB; 1994.

[21] Ockleston A. Arching action in reinforced concrete slabs. The Structural Engineer. 1958;36:197-201.

[22] Wood RH, Drucker DC. Plastic and Elastic Design of Slabs and Plates. Journal of Applied Mechanics. 1961;30:159-.

[23] PARK R. ULTIMATE STRENGTH OF RECTANGULAR CONCRETE SLABS UNDER SHORT-TERM UNIFORM LOADING WITH EDGES RESTRAINED AGAINST LATERAL MOVEMENT. Proceedings of the Institution of Civil Engineers. 1964;28:125-50.

[24] Chen W, Luo L, Guo Z, Yuan P. Experimental studies on load-carrying capacity of HFR-LWC beams accompanying membrane action. Engineering Structures. 2021;228:111497.

[25] Chen L, Fang Q, Guo Z, Liu J. An improved analytical method for restrained RC structures subjected to static and dynamic loads. International Journal of Structural Stability and Dynamics. 2014;14:1350052.

[26] Dat P, Tan K-H. Membrane actions of RC slabs in mitigating progressive collapse of building structures. Engineering Structures - ENG STRUCT. 2011;55.

[27] Qian K, Li B, Ma J-X. Load-Carrying Mechanism to Resist Progressive Collapse of RC Buildings. Journal of Structural Engineering. 2015;141:04014107.

[28] Qian K, Li B. Performance of Three-Dimensional Reinforced Concrete Beam-Column Substructures under Loss of a Corner Column Scenario. Journal of Structural Engineering. 2013;139:584-94.

[29] Qian K, Geng S-Y, Liang S-L, Fu F, Yu J. Effects of loading regimes on the structural behavior of RC beam-column sub-assemblages against disproportionate collapse. Engineering Structures. 2022;251:113470.

[30] Park R. Tensile membrane behaviour of uniformly loaded rectangular reinforced concrete slabs with fully restrained edges. Magazine of Concrete Research. 1964;16:39-44.

[31] Li Q, Jones N. Shear and adiabatic shear failures in an impulsively loaded fully clamped beam. International Journal of Impact Engineering - INT J IMPACT ENG. 1999;22:589-607.

[32] Xu J, Wu C, Li Z-X. Analysis of direct shear failure mode for RC slabs under external explosive loading. International

Journal of Impact Engineering. 2014;69:136-48.

[33] Subramanian N. Design of reinforced concrete structures: Oxford University Press; 2013.

[34] AS3600-2018. Concrete Structures. Standards Australia Limited. Sydney. 2018.

[35] Bentz EC. Sectional analysis of reinforced concrete members: University of Toronto Toronto; 2000.

[36] CSA A23.3-2004. Design of concrete structure. Canadian Standards Association. 2004.

[37] ACI Committee. Building code requirements for structural concrete (ACI 318-14) and commentary. American Concrete Institute; 2014.

[38] Chen C, Cheng L. Single Crack-Based Model for FRP Shear-Strengthened RC Beams. Journal of Composites for Construction. 2019;23:04019030.